수평으로 회전하는 실린더 내부의 테흐름의 형태에 대한 실험 및 수치해석적 연구

배선혁, 김도현
한국과학기술원 생명화학공학과, 초미세화학공정시스템 연구센터

Experimental and computational study on the patterns of rimming flow within a rotating horizontal cylinder

Sun Hyuk Bae and Do Hyun Kim
Department of Chemical and Biomolecular Engineering & Center for Ultramicrochemical Process Systems, Korea Advanced Institute of Science and Technology, Daejeon 305-701, Korea

Introduction

Rimming flow is the coating flow of a thin liquid layer at the inside surface of a horizontally rotating cylinder and has been observed experimentally by many researchers. Rimming flow shows various unstable patterns as the rotating speed changes. Since this dissipative system is nonlinear and far from the equilibrium, it is appeared obscure how such unstable patterns are formed. However, there have been several researches dealing with the lubrication analysis or numerical computation mainly concentrating on the flow instability or thickness profile of the free surface to perform a systematic analysis of rimming flow[1-5]. Here, the purpose of this research is to analyze the deformation of the free surface location and visualize the pressure and the flow field according to the variation of the several process parameters. The numerical analysis was performed by Galerkin finite element method in 2-D cross sectional geometry with solving the Navier-Stokes equation. As a result, we classified the homogeneous film and bump state by observing the change of the arc length of the free surface according to the dimensionless parameter β which is the ratio of gravity to viscosity.

Flow geometry and numerical method

The calculations are for steady, 2-D cross-sectional, continuous liquid films with specified parameters. Fig. 1 shows the schematic geometry of rimming flow in a bump state. Fluid flow within the domain is described by the incompressible Navier-Stokes equations for a Newtonian fluid and continuity equation. At the cylinder surface, no slip boundary condition yields and at the gas/liquid interface of steady state rimming flow, kinematic boundary condition that means no liquid cross the interface is applied and the conservation conditions of momentum which are the shear and normal stress balances is applied. According to the formulation used by Sackinger *et al.*[6], the gas pressure is set arbitrarily and the datum pressure is computed using the volume constraint for steady flows.

Governing equations are discretized by Galerkin finite element method. Total unknowns of interest are $\boldsymbol{u}$, p, h and P_g. Newton-Raphson method is used to reformulate the discretized nonlinear equations into linear matrix equations which in turn are calculated by frontal solver. For the calculation of the free surface deformation, we used spine method developed by Saito and Scriven[7], wherein mesh nodes that are free to move lie on the generator lines called spines. After each Newton iteration, the new nodal value of free surface location is updated to reform the mesh.

Experimental setup

Our experimental apparatus is similar to that used in the previous work[4] except that the radius of circular Plexiglas cylinder is 2.5cm and the axial length is 35cm. Moreover, we introduced belt type rotating system with off-axis between the motor and the cylinder instead of shaft connecting motor to the one end side of the cylinder, in order to facilitate the observation of 2-D cross sectional free surface shape in the axial direction. We used silicone oil(dimethylpolysiloxane, Shin-Etsu Chemical Co.) with various viscosity (100 ~ 5000cSt). The surface tension of the fluid is 21dyn/cm at 25℃. This oil ensures a perfect wetting on the Plexiglas substrate. We confirmed that there is little capillary rise at the solid-liquid interface between the end caps and fluid and actually we had a sufficiently clear view without any optical difficulty. By taking a photograph with a high resolution digital camera, we measured the free surface location along azimuthal direction by means of image processing program. The range of rotating speed of cylinder and fluid filling fraction are 2 ~ 150rpm and 0.1 ~ 0.3, respectively, which are same to those used in numerical computation.

Results and discussion

When gravity is ignored, the free surface shows a concentric shape and the constant film thickness is controlled only by fluid filling fraction. And the dynamic pressure shows maximum on the free surface and minimum on the rotating cylinder surface. The velocity field shows a similar pattern to a typical concentric Couette flow except one thing that the radial directional velocity profile shows linearly increasing shape in our case.

With gravity, the rimming flow patterns can be classified typically into three types as shown in Fig. 2. Usually the rimming flow film is thicker at the rising side and thinner at the falling side when the film is homogenous as shown in Fig. 2(a). When the rotating speed decreases the bump starts to appear as shown in Fig. 2(b). It is observed that the bump starts to appear at the region of $1.5\pi < \theta < 2\pi$ as a small convex and it moves down to the center of the cylinder bottom. If the rotating speed decreases more than that of the bump state, the bump shape disappears and the free surface shows nearly horizontal shape at the cylinder bottom as shown in Fig. 2(c). And we could observe the novel phenomena that the secondary recirculation flow whose direction is reverse to the first one in bump state appears and becomes as large as the first one as the rotating speed decreases. We called this state as the secondary recirculation state. Moreover, at the left side of the secondary recirculation flow we could observe another recirculation flow which is small in size and the direction of which is same to the first one.

The changes of the free surface shape from homogenous film, bump to secondary recirculation state as shown in Fig. 2 could also be observed by the increase of the fluid filling fraction or the decrease of the fluid viscosity. Fig. 3(a) and Fig. 3(b) show the effects of the fluid filling fraction and the fluid viscosity. We could observe similar homogenous films when the fluid filling fraction is low (F=0.1) or viscosity is high (μ=5000cP) and the secondary recirculation flows when F=0.3 or μ=100cP as well as the bump shapes for the residual parameters.

For scaling the importance of gravity and viscosity, it is usual to use the dimensionless parameters such as Stokes number, which can be expressed as Fr/Re=$Rg/\Omega\nu$ where Fr is Froude number. By modifying the Stokes number with combining fluid filling fraction F, we can get the dimensionless parameter β as,

$$\beta = F\sqrt{\mathrm{St}} = F\sqrt{\frac{gR}{\Omega\nu}} \tag{1}$$

By substituting the parameters F, Ω and ν with β, we traced the change of the arc length of the free surface as shown in Fig. 3(c). We could observe that the arc length maintains constant when β is small. This region is where the rotating speed or viscosity is high enough to form the homogenous film that the shape of free surface does not change noticeably according to the variation of the parameters. These onset values are all in the range of 1.4 and 1.6, which correspond to that of the previous experimental work[4] which was 1.414. But when β is larger than those critical values, arc length starts to decrease abruptly, which means the formation of the bump.

It is well anticipated that the surface tension becomes dominant around the ridge of the bump due to the large curvature. Therefore we observed that the variation of the surface tension changes the flow states and affects on the critical β values on transitions. Fig. 4 shows the steady rimming flow regimes in a numerically calculated phase diagram in a Ca-β space, showing the regions of homogeneous film and bump states for F=0.3. Dashed line is when β is 1.586. We observed that the critical Ca value for the onset of transition from homogenous film to bump decreases as β increases. If F is varies also does the critical Ca value but the decreasing tendency is maintained.

The comparison of our results to the recent computational works performed by Hosoi and Tirumkudulu is plotted in Fig. 4(b) for F=0.13, Ω=46.79rpm, μ=485cP and R=5cm. There is good agreement among all the three works except the region which is shown in the inset. And we compared the computational result to our experimental one which is shown in Fig. 4(c) for F=0.3, Ω=18rpm, μ=485cP and R=2.5cm. It is shown that the results are matching well each other except the small difference at bump region.

In conclusion, we have considered the change of the free surface shape depending on various conditions in a partially-filled horizontal rotating cylinder by performing Galerkin finite element analysis to solve the Navier-Stokes equation. We observed the pressure, velocity field and shear rate as the free surface shape changes from homogeneous film, bump to secondary recirculation states. And with the dimensionless parameter β, we confirmed the onset condition for the transitions between three states by observing the change of the arc length of the free surface. Our computational results matched well with those obtained experimentally and obtained by lubrication analysis of the previous works.

Acknowledgements

The authors wish to acknowledge the support by the BK 21 project and this research was partially funded by Center for Ultramicrochemical Process Systems sponsored by KOSEF.

References

1. F. Melo, *Phys. Rev. E*, **48**, 2704 (1993).
2. R. E. Johnson, *J. Fluid Mech.*, **190**, 321 (1988).
3. A. E. Hosoi and L. Mahadevan, *Phys. Fluids*, **11**, 97 (1999).
4. M. Tirumkudulu and A. Acrivos, *Phys. Fluids*, **13**, 14 (2001).
5. R. T. Balmer, *Nature(London)*, **227**, 600 (1970).
6. P. A. Sackinger, R. A. Brown, and J. J. Derby, *Intl. J. Numer. Meth. Fluids*, **9**, 453 (1989).
7. H. Saito and L. E. Scriven, *J. Comput. Phys.*, **42**, 53 (1981).

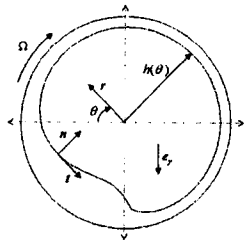

Figure 1. 2-D cross-sectional schematic geometry of the rimming flow with a bump.

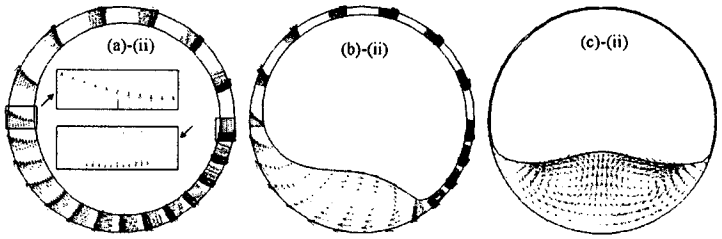

(a) (b) (c)

Figure 2. Three types of rimming flow patterns; (a) homogenous film at 150rpm, (b) bump at 50rpm and (c) secondary recirculation flow at 2 rpm.

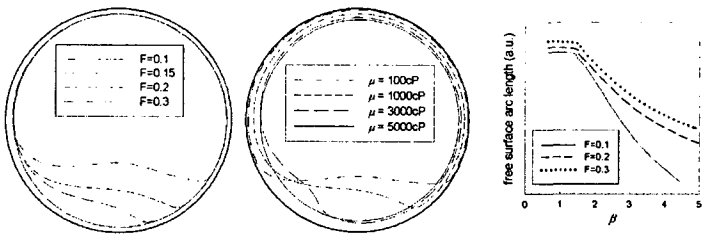

(a) (b) (c)

Figure 3. Effects of (a) the fluid filling fraction change and (b) the fluid viscosity change on the free surface shape. (c) Free surface arc length change according to a rotating speed variation for μ=485cP.

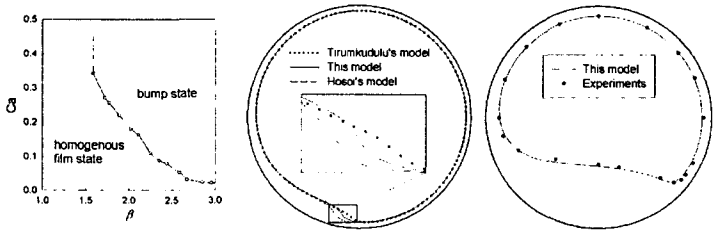

(a) (b) (c)

Figure 4. (a) Numerically calculated phase diagram showing the region of the homogenous film, bump and secondary recirculation state for F=0.3. Comparison of our computational results to (b) the recent computational works by Hosoi and Tirumkudulu for F=0.13, Ω=46.79rpm, μ=485cP and R=5cm and (c) our experimental one.